Chinese Chemical Letters 37 (2026) 111496

Contents lists available at ScienceDirect

Chinese Chemical Letters

journal homepage: www.elsevier.com/locate/cclet

Hollow mesoporous Prussian blue nanozymes with intrinsic self-chromogenicity and photothermal amplification as a pH-adaptive dual-modal biosensor for one-step glucose monitoring

Mingyue Luo[a], Xin Xue[b], Kehui Zhang[c], Honghong Rao[c], Baodui Wang[b], Zhentong Zhu[a], Jinhai Fan[d], Zhonghua Xue[a,*]

[a] Key Laboratory of Water Security and Water Environment Protection in Plateau Intersection (NWNU), Ministry of Education, College of Chemistry & Chemical Engineering, Northwest Normal University, Lanzhou 730070, China
[b] State Key Laboratory of Applied Organic Chemistry and Key Laboratory of Nonferrous Metal Chemistry and Resources Utilization of Gansu Province, Lanzhou University, Lanzhou 730000, China
[c] School of Chemical Engineering, Lanzhou City University, Lanzhou 730070, China
[d] Department of Urology, The First Affiliated Hospital of Xi'an Jiaotong University, Xi'an 710061, China

ARTICLE INFO

Article history:
Received 31 March 2025
Revised 19 June 2025
Accepted 19 June 2025
Available online 21 June 2025

Keywords:
Hollow mesoporous Prussian blue nanozymes
Multicolorimetric modal
Photothermometric modal
Enzyme-nanozymes cascade assays
One-step detection

ABSTRACT

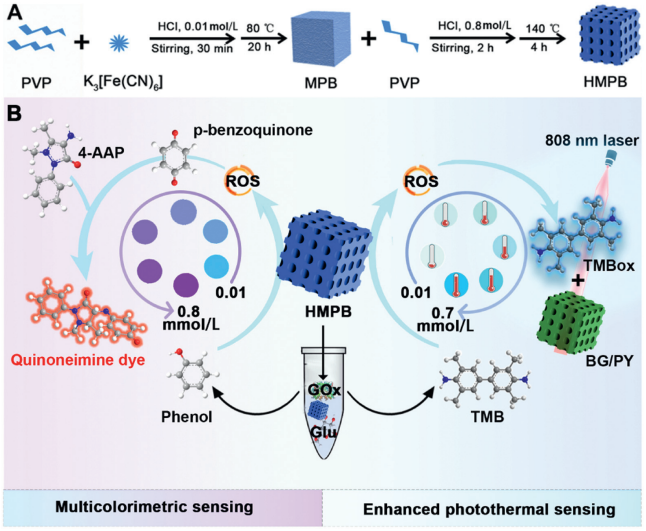
Traditional enzyme-nanozymes cascade assays for glucose detection are usually limited by pH incompatibility and operational complexity. Herein, we present a strategy based on hollow mesoporous Prussian blue (HMPB) nanozymes for one-step, dual-modal glucose sensing under neutral conditions. The rationally designed HMPB nanozymes exhibit intrinsic peroxidase-like activity at physiological pH (~7.4), inherent chromogenic properties and superior photothermal conversion efficiency. These features directly enable integration with glucose oxidase (GOx) for one-step glucose detection without intermediate pH adjustment. Additionally, the catalytic coupling of 4-aminoantipyrine/phenol oxidation products, enhanced by the intrinsic blue coloration of HMPB, generates vivid multicolorimetric responses for smartphone-based quantitative analysis. To enhance signal reliability, the photothermal properties of HMPB nanozymes are further ingeniously coupled with the thermal-responsive characteristics of oxidized 3,3′,5,5′-tetramethylbenzidine (oxTMB), establishing a dual-amplified thermal imaging platform through portable infrared thermal imager detection. HMPB nanozymes serve as both a catalytic activator and an intrinsic signal reporter, establish a new platform in dual-modal glucose monitoring. The platform demonstrates remarkable clinical adaptability through its smartphone-compatible colorimetric readout and portable thermal imaging capabilities, achieving a detection limit of 1.39 μmol/L (multicolorimetric modal) and 3.05 μmol/L (photothermometric modal) for glucose with robust reliability in human serum samples. This research overcomes the pH mismatch barrier in enzyme-nanozymes cascade system, and providing a cost-effective, instrument-flexible detection strategy that bridges laboratory research and point-of-care diagnostics.

© 2025 Published by Elsevier B.V. on behalf of Chinese Chemical Society and Institute of Materia Medica, Chinese Academy of Medical Sciences.

Glucose monitoring is indispensable in clinical diagnostics and chronic disease management, where enzymatic cascade systems based on glucose oxidase (GOx) and horseradish peroxidase (HRP) long serving as the gold standard [1,2]. However, the intrinsic limitations of natural enzymes, such as poor thermal stability, stringent storage requirements, and high production costs, impede their scalability for point-of-care testing (POCT) [3,4]. Therefore, nanozymes with peroxidase (POD)-like activity have emerged as promising alternatives due to their robust stability, tunable catalytic properties, and cost-effectiveness, to fabricate enzyme-nanozymes cascade systems for glucose detection for addressing the limitations of natural enzymes based cascade systems [5,6]. Unfortunately, most existing enzyme-nanozymes cascade systems for glucose detection remain constrained by a fundamental incompatibility: The acidic pH optimum (pH 3–4) of most POD-like nanozymes clashes with the neutral physiological pH (~7.4) required for GOx activity [7,8]. This mismatch necessitates laborious multi-step pH adjustments during assays [9–11], leading to operational complexity and dilution-induced inaccuracies that critically undermine the simplicity and reliability required for POCT.

* Corresponding author.
E-mail address: xzh@nwnu.edu.cn (Z. Xue).

https://doi.org/10.1016/j.cclet.2025.111496
1001-8417/© 2025 Published by Elsevier B.V. on behalf of Chinese Chemical Society and Institute of Materia Medica, Chinese Academy of Medical Sciences.



Scheme 1. (A) The synthetic flow of the proposed HMPB nanozymes. (B) One-step and dual-modal glucose detection based on multifunctional HMPB nanozymes system under neutral conditions.

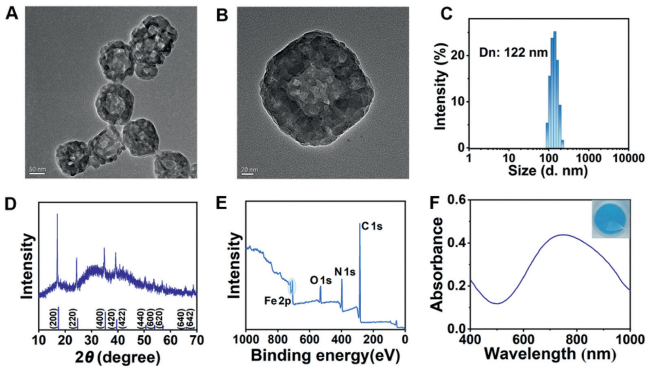


Fig. 1. Characterization of the synthesized HMPB. (A) TEM image, (B) HRTEM image, (C) DLS measurements, (D) XRD spectra, (E) XPS survey spectra, (F) UV–vis absorption spectra and the photo of the solution (inset).

Yet, efficient, one-pot multi-step catalytic reactions are still quite rare due to compatibility of the reaction conditions of different steps [12–14]. It therefore is essential to employ nanozymes with high intrinsic activity under neutral conditions. For example, Liu *et al.* demonstrate an effective bio-nanozyme cascade formed by GOx and *in situ*-generated nanoceria, which can be used for one-pot detection of glucose in serum under physiological conditions [12]. Despite recent advancements, most existing enzyme-nanozymes cascade platforms rely on single-signal outputs (*e.g.*, colorimetric, fluorometric or surface-enhanced Raman scatting), which are inherently vulnerable to environmental interferences or instrumental variability. This signal singularity raises concerns about false-positive/negative readings, particularly in complex biological matrices like serum, where coexisting substances may perturb detection specificity. It therefore is worth noting that the introduction of multifunctional nanozymes holds promise for reliable dual/multi-modal glucose detection [15,16]. For instance, Wu's group developed a dual-modal (colorimetric and fluorometric) detection method for the detection of glucose based on the multifunctional iron-doped carbon dots nanozymes [15]. Although this dual-modal strategy improved detection reliability, but their widespread application is hindered due to the lack of signal enhancement strategies and the difficulty in synchronously enhancing multiple signals.

Prussian blue analogs (PBAs) present a unique solution to these challenges through their intrinsic multifunctionality [17]. Beyond demonstrating excellent POD-like activity, PBAs exhibit distinctive chromogenic properties and exceptional photothermal conversion efficiency [18,19]. Capitalizing on these characteristics, we synthesized and engineered a hollow mesoporous Prussian blue (HMPB) nanocubes based system for one-step and dual-modal sensing glucose under neutral conditions. The HMPB nanocubes were fabricated based on a simple hydrothermal method by etching mesoporous Prussian blue with hydrochloric acid (Scheme 1A). Specifically, as shown in Scheme 1B, the system operates via one-step enzyme-nanozymes cascade system: (1) GOx-generated H_2O_2 activates HMPB's POD-like activity under neutral conditions to catalyze 4-AAP/phenol oxidation, generating red quinone dyes that synergize with HMPB's intrinsic blue coloration for establishing a self-chromogenic multicolorimetric response readout. (2) HMPB-catalyzed TMB oxidation and integrating the intrinsic photothermal properties of HMPB nanozymes generating an enhanced photothermometric response readout. By eliminating pH adjustments and integrating dual signal modalities, this platform overcomes traditional enzyme-nanozymes cascade limitations of multi-step operations and physiological incompatibility. This work establishes a new biosensing paradigm where HMPB multifunctional nanozymes serve dual roles both as a catalytic activator and an intrinsic signal reporter, bridging laboratory research to point-of-care diagnostics through instrument-flexible smartphone and thermal camera readouts.

HMPB nanozymes were synthesized through hydrothermal etching of mesoporous Prussian blue (MPB) precursors. Transmission electron microscopy (TEM) analysis (Fig. 1A, Figs. S1B and C in Supporting information) revealed morphological evolution during the etching process. The critical parameters in the synthesis process of HMPB, such as HCl concentration, PVP amount, and hydrothermal time, were briefly discussed in terms of how they influence nanozyme activity and morphology (Fig. S2 in Supporting information). It was ultimately determined that with an HCl concentration of 0.8 mmol/L, a PVP amount of 100 mg, and an etching time of 4 h, HMPB maintains its cubic morphology while displaying a distinct hollow structure with substantial internal cavities after etching (Fig. 1B). Dynamic light scattering (DLS) measurements confirmed favorable colloidal stability with an average hydrodynamic diameter of 122 nm (Fig. 1C). Crystalline structure analysis *via* X-ray diffraction (XRD) exhibited characteristic HMPB diffraction peaks at 17.5°, 24.4°, 34.8°, and 39.2°, attributed to the (200), (220), (400), and (420) diffraction planes of PB crystals (JCPDS PDF #52–1907) (Fig. 1D). The chemical functionalization was systematically verified through FTIR spectral interrogation (Fig. S3 in Supporting information). Two characteristic absorption bands were identified: The cyanide bridging ligand's C≡N stretching mode (2082 cm^{-1}) and the amide carbonyl (C=O) stretching vibration from polyvinylpyrrolidone (PVP) macromolecules (1646 cm^{-1}) [20]. This evidence conclusively demonstrates successful PVP encapsulation on the HMPB nanozymes surface. X-ray photoelectron spectroscopy (XPS) survey scan (Fig. 1E) identified Fe, C, N, and O constituents, with high-resolution Fe 2p spectrum resolving two pairs of doublets identified as Fe $2p_{1/2}$ and $2p_{3/2}$. Further peak deconvolution indicates that distinct peaks at 708.5 eV and 721.5 eV are attributed to Fe^{2+}, whereas the less intense peaks at 712.7 eV and 725.0 eV correspond to Fe^{3+}, signifying the presence of Fe^{2+}/Fe^{3+} species on the surface of the HMPB nanozymes (Fig. S4 in Supporting information) [21]. Optical characterization showed broad NIR absorption (750 nm peak) (Fig. 1F). HMPB nanozymes maintained good solution stability and enzyme-like activity under different solution and humidity conditions (Figs. S5 and S6 in Supporting in-

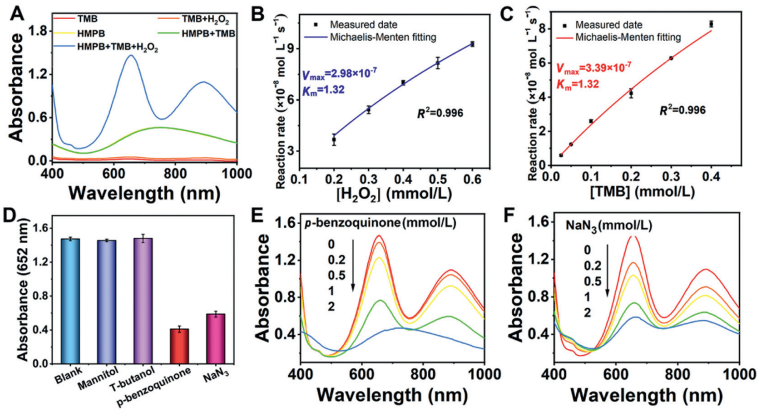


Fig. 2. (A) UV–vis spectra of HMPB nanozymes system with different components. Steady-state kinetic assay of HMPB nanozymes with H_2O_2 (B) and TMB (C) as substrates. (D) The absorbance intensity at 652 nm of HMPB nanozymes system with different ROS scavengers. The absorption spectra of HMPB nanozymes system with different concentrations of (E) *p*-benzoquinone and (F) NaN_3. Data are presented as mean ± SD ($n = 3$).

formation). All these observations collectively validate the successful fabrication of HMPB nanozymes.

To substantiate the enzyme-mimetic activity of the synthesized HMPB nanozymes, a chromogenic assay system was established using TMB as prototypical peroxidase substrate [22]. As demonstrated in Fig. 2A, the characteristic absorption at 652 nm, indicative of oxidized TMB (oxTMB) formation, emerged exclusively in the presence of both HMPB nanozymes and H_2O_2. Control experiments revealed no detectable chromogenic conversion when H_2O_2 was omitted from the reaction system. This confirms the H_2O_2-dependent POD activity of HMPB nanozymes. To elucidate the catalytic kinetic mechanism of HMPB nanozymes, steady-state kinetics were conducted using the common nanozymes substrates TMB and H_2O_2 at varying concentrations [23]. The obtained data aligned well with the Michaelis-Menten equation, allowing for the calculation of the Michaelis-Menten constant (K_m) and maximum reaction velocity (V_{max}) (Figs. 2B and C). The K_m and V_{max} values indicate the substrate affinity for the enzyme and the enzyme's turnover number, respectively [24]. As well known, lower K_m and higher V_{max} indicate a higher affinity and conversion efficiency of enzyme for the substrate. The K_m values were in this tested system determined to be 1.32 mmol/L for H_2O_2 and TMB, suggesting that HMPB nanozymes possess high affinity for both substrates. The V_{max} values were recorded as 2.98×10^{-7} mol L^{-1} s^{-1} for H_2O_2 and 3.39×10^{-7} mol L^{-1} s^{-1} for TMB, which exceed those of several previously studied nanozymes [25,26], strongly supporting an excellent enzyme-mimetic activity of the prepared nanozymes. To elucidate the reactive species involved in the HMPB nanozymes-catalyzed reaction, a systematic scavenger study was conducted using specific quenchers (Fig. 2D): Mannitol and *t*-butanol for hydroxyl radicals (•OH), *p*-benzoquinone for superoxide radicals ($O_2^{\bullet-}$), and sodium azide (NaN_3) for singlet oxygen ($^1O_2$) [27]. Dose-dependent suppression (Figs. 2E and F) showed progressive activity reduction with increasing *p*-benzoquinone (0–2 mmol/L) and NaN_3 (0–2 mmol/L) concentrations, while hydroxyl radical scavengers (mannitol/*t*-butanol) exhibited negligible effects. These results conclusively demonstrate $O_2^{\bullet-}$ and $^1O_2$ as dominant reactive oxygen species governing the nanozyme's catalytic mechanism.

The inherent strong blue coloration of HMPB nanozymes provides a unique optical reference for constructing multicolorimetric sensing systems, significantly enhancing visual resolution in point-of-care testing (POCT) applications [28]. Initial attempts in this study to integrate green chromogenic components through ABTS oxidation proved ineffective, as HMPB nanozymes exhibited negligible oxidative capacity toward ABTS under neutral to near-neutral conditions (pH 6.5–7.4), with only marginal activity observed at pH 5.5 (Fig. S7 in Supporting information). This limitation prompted exploration of alternative chromatic systems. Inspiration from classical phenol-4-aminoantipyrine (4-AAP) chemistry revealed a viable pathway for red chromophore generation [29,30]. While traditional methods employ potassium ferricyanide as the oxidant (Fig. S8 in Supporting information), we successfully substituted this with enzymatically generated H_2O_2 through a cascade reaction involving glucose oxidase (GOx)-mediated glucose hydrolysis [31]. As illustrated in Fig. 3A, this innovation enabled a one-step detection platform where HMPB nanozymes catalyze H_2O_2-driven oxidative coupling of 4-AAP and phenol, producing a distinct chromatic transition from blue to purple and subsequently to magenta. Critical optimization studies demonstrated exceptional pH adaptability, with maximum colorimetric response at physiological pH (7.0) and sustained high efficiency under alkaline conditions (Fig. 3B). This represents a significant advancement over conventional quinoneimine-based systems that typically require acidic environments [32]. Although complementary color theory suggested potential utility of orange chromophores via o-phenylenediamine (OPD) oxidation, practical implementation revealed background interference from spontaneous HMPB-mediated OPD oxidation in the absence of H_2O_2 (Fig. S9 in Supporting information), precluding reliable target quantification. The developed platform synergistically combines HMPB's intrinsic optical properties with rationally designed chromatic transitions, achieving enhanced visual discrimination while maintaining operational simplicity critical for resource-limited settings.

The analytical performance of the H_2O_2 sensing system was systematically optimized by investigating key reaction parameters (Fig. S10 in Supporting information). Under optimal conditions, the sensor exhibited dual linear detection ranges of 0.01–0.05 mmol/L ($A_{506} = 6.314C + 0.284$, $R^2 = 0.994$) and 0.05–0.7 mmol/L ($A_{506} = 2.434C + 0.529$, $R^2 = 0.998$), with detection limits of 1.87 μmol/L and 4.85 μmol/L ($3\sigma/k$, σ represents the standard deviation of 20 blank samples, and k represents the slope of the standard curve), respectively. The chromatic transition from blue to magenta provided intuitive visual confirmation of H_2O_2 quantification (Fig. S11A in Supporting information). The interference of amino acids, reducing agents, and ions was investigated (Figs. S12 and S13 in Supporting information). Under the presence of masking agents, the robustness of the system in complex biological samples was confirmed (Fig. S14 in Supporting information).

The multicolorimetric detection system (Fig. 3A) functions *via* a dual-enzymatic cascade: GOx first converts glucose to gluconic acid with H_2O_2 generation, followed by HMPB nanozymes-catalyzed oxidative coupling of phenol and 4-AAP to produce

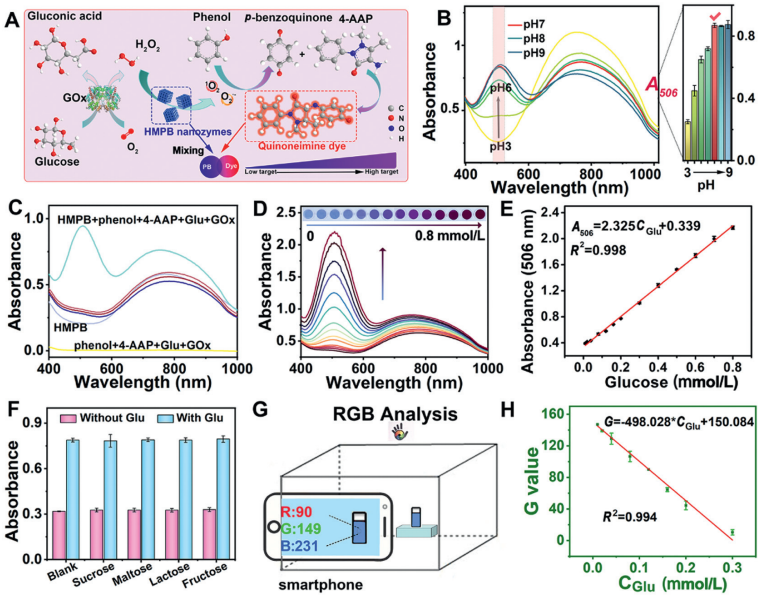


Fig. 3. (A) Schematic diagram of the one-pot multicolorimetric method for the detection of H_2O_2 and glucose. (B) The catalytic activity of HMPB nanozymes for 4-AAP/phenol oxidation at different pH. (C) glucose detection feasibility analyses corresponding to UV–vis spectra. (D) The absorption spectra of glucose at concentrations of 0–0.8 mmol/L were present. (E) Correlation between A_{506} and glucose concentration. (F) Selectivity experiment for detecting glucose (Glu: 200 μmol/L, Interferents: 2 mmol/L). (G) Schematic diagram of glucose concentration detection by smartphone. (H) plot of G value *vs.* the concentration of glucose. Data are presented as mean ± SD ($n = 3$).

red quinoneimine chromophores. This process induces glucose concentration-dependent chromatic transitions from HMPB's intrinsic blue to purple hues, with visual gradients correlating to analyte levels. Control experiments (Fig. 3C) verified system specificity—no chromogenic response occurred with isolated GOx or glucose alone. Distinct 506 nm absorbance and purple coloration emerged exclusively in complete systems containing both enzymes and glucose, confirming H_2O_2's essential role as a signaling mediator. This cascade design ensures selective glucose detection by coupling enzymatic specificity to nanozyme activity, effectively mitigating interference from biological matrix components.

To achieve optimal detection performance of glucose, systematic optimization of enzymatic parameters was conducted (Fig. S15 in Supporting information). The system exhibited distinct chromatic transitions from blue to purple and ultimately magenta across increasing glucose concentrations (0–0.8 mmol/L), as illustrated in Fig. 3D inset. Quantitative analysis revealed a linear correlation ($A_{506} = 2.325C_{Glu} + 0.339$, $R^2 = 0.998$) across the clinically relevant 0.01–0.8 mmol/L range (Fig. 3E). The calculated limit of detection (1.39 μmol/L, $3\sigma/k$) address critical needs for early-stage hyperglycemia identification and precise glycemic control. Control experiments with 2000 μmol/L interfering saccharides (lactose, maltose, sucrose, fructose) *versus* 200 μmol/L glucose revealed selective 506 nm absorbance enhancement exclusively in glucose samples (Fig. 3F), demonstrating the platform's excellent selectivity for glucose detection against structurally similar saccharides.

To enhance field applicability, we developed a smartphone-integrated detection platform combining chromatic signal capture with computational analysis. The system features a standardized imaging chamber (Fig. 3G) that minimizes environmental interference. Smartphone-captured RGB analysis of the HMPB-phenol-4-AAP system revealed concentration-dependent chromatic shifts (0–0.8 mmol/L glucose), with green (G) and blue (B) channels showing significant decreases (Fig. S16 in Supporting information). The G channel demonstrated superior linearity ($R^2 = 0.994$) in the 0.01–0.3 mmol/L range ($G = 150.084 - 498.028C_{Glu}$), achieving a detection limit of 2.51 μmol/L (Fig. 3H). Complementary B channel analysis showed linear response up to 0.6 mmol/L (Fig. S17 in Supporting information). This integration of smartphone technology with nanozyme-based detection enables precise, equipment-free glucose quantification suitable for resource-limited settings.

During the investigation of the multicolorimetric sensing platform, we observed notable alterations in the characteristic UV–vis absorption peak of HMPB nanozymes at 750 nm (Fig. 3D and Fig. S8). Specifically, these ROS participate not only in substrate oxidation but also undergo self-redox reactions mediated by the multivalent iron centers (Fe^{2+}/Fe^{3+}) within the HMPB crystalline framework [17]. To validate the universality of this phenomenon, we employed *o*-phenylenediamine (OPD) as an alternative enzymatic substrate. As depicted in Fig. S18 (Supporting information), progressive elevation of glucose concentrations induced concurrent enhancement of absorption peaks at 420 nm (corresponding to OPD oxidation products, oxOPD) and 750 nm, demonstrating similar behavior to the 4-AAP/phenol-based oxidation system. This observation aligns with previous reports regarding the redox reversibility of HMPB-based nanosystems [17]. The reversible transition between PB and its reduced form (Prussian white, PW) was mediated by ascorbic acid (AA) as a reductant and potassium permanganate as an oxidant, respectively (Fig. S19A in Supporting information). Given the strong near-infrared (NIR) absorption of HMPB nanozymes, we explored their potential for photothermal sensing applications. Under NIR irradiation, the nanozymes induced a significant temperature increase of 8.2 °C, which was modulated by redox interactions. AA-mediated reduction lowered the temperature increment to 5.2 °C, corresponding to decreased absorption at 750 nm. The HMPB framework demonstrated multi-stage redox transitions, including conversions among PB, PW, Berlin green (BG), and Prussian yellow (PY) under oxidative conditions (Fig. 4A). The introduction of permanganate restored both NIR absorption and photothermal response, confirming the system's reversibility (Fig. S19 in Supporting information). While the intrinsic photothermal properties of HMPB enable temperature-based detection, the limited signal dynamic range may constrain sensitivity for trace analyte detection. Remarkably, the oxidation product of TMB (oxTMB) exhibits dual advantages as a chromogenic probe and photothermal transducer, demonstrating prominent absorption

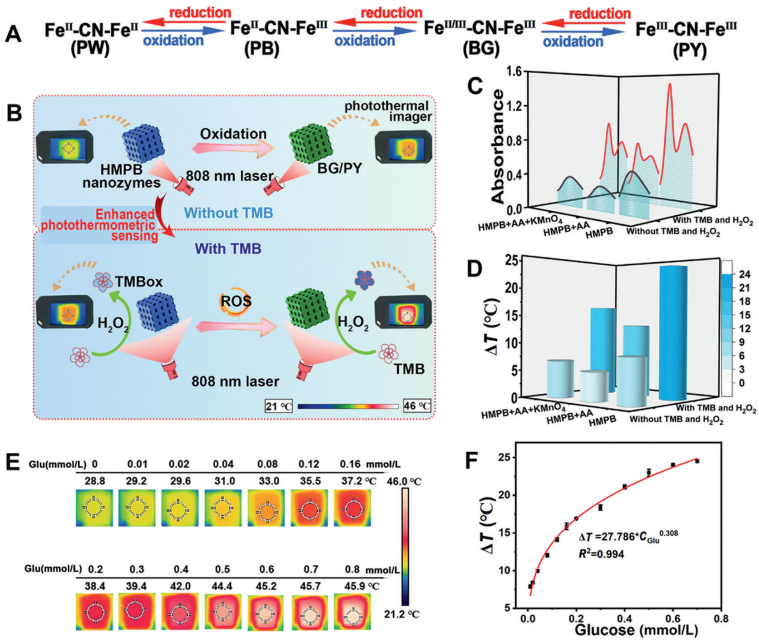


Fig. 4. Schematic diagram of (A) the conversion of Prussian blue materials containing different valence states of Fe. and (B) integrating a dual thermal signal platform based on HMPB nanozymes. (C) UV–vis absorption spectra and (D) bar plot of temperature changes of AA/$KMnO_4$ added to HMPB nanozymes system. (E) Infrared image of the system containing different concentrations of glucose irradiated by 808 nm laser with power density of 4 W/cm^2 for 240 s. (F) Corresponding calibration curves. Data are presented as mean ± SD ($n = 3$).

peaks at 650 nm and 894 nm. This discovery prompts us to propose an optimized sensing paradigm that synergistically integrates the photothermal properties of HMPB nanozymes with the thermal responsiveness of oxTMB, establishing a dual-amplified thermal imaging platform with enhanced signal reliability through portable infrared thermal imager detection (Fig. 4B). The actual detection process is shown schematically in Fig. S20 (Supporting information).

To validate the feasibility of this photothermal sensing, we first conducted proof-of-concept experiments (Figs. 4C and D). While the POD-like activity of HMPB nanozymes induced significant UV–vis absorption enhancement upon interaction with TMB and H_2O_2, quantitative integration of absorbance data for enhanced sensing proved unfeasible due to spectral incompatibility. By synergistically combining the photothermal properties of HMPB nanozymes and the thermal response of oxTMB, we established a photothermal detection platform with dual thermal signals amplified readout. As shown in Fig. 4D, the HMPB nanozymes-TMB-H_2O_2 system achieved a remarkable 24.0 °C temperature elevation under NIR irradiation, demonstrating superior photothermal conversion efficiency. AA introduction reduced this increment to 13.2 °C, substantially greater than HMPB's standalone response. These results confirm that target-induced modulation of HMPB nanozymes's POD-like activity can be amplified through dual photothermal signal integration, thereby enabling the construction of a highly responsive temperature-based sensing platform.

To optimize the photothermal sensing performance, we investigated the NIR-driven photothermal characteristics of HMPB nanozymes and optimized the concentration of the substrate TMB (Fig. S21 in Supporting information). The quantitative analytical performance was evaluated using thermal imaging as signal readout with varying glucose concentrations (0.01–0.7 mmol/L). Thermal images exhibited progressive color transition from yellow through red to white (Fig. 4E), corresponding to concentration-dependent temperature increments. As shown in Fig. 4F, quantitative analysis revealed an exponential relationship between ΔT and glucose concentration: $\Delta T(°C) = 27.786 C_{Glu}{}^{0.308}$ ($R^2 = 0.994$). This system achieved a detection limit of 3.05 μmol/L ($3\sigma/k$). Comparative analysis with established glucose detection methods (Table S1) confirmed the high sensitivity of our multicolorimetric and photothermometric methods, while maintaining operational simplicity.

To validate the clinical applicability of this method, multicolorimetric and photothermometric glucose detection in human serum samples were conducted. Undiluted serum aliquots (10 μL) were directly introduced into the reaction system without any pretreatment, simulating clinical testing conditions. As summarized in Table S2 (Supporting information), both detection modals demonstrate excellent diagnostic reliability, with measured glucose levels for five clinical samples, showing excellent concordance with commercial glucometer readings. The methodologies exhibited good consistency, yielding relative standard deviations (RSD) below 5.56 % across all serum analyses. These results underscore the applicability, accuracy and feasibility of the one-step assay for clinical use. Furthermore, the repeatability and stability of the proposed dual-modal glucose sensing platform was demonstrated (Fig. S22 in Supporting information). In summary, the demonstrated sensitivity, accuracy, and operational simplicity affirm the potential of this detection platform for practical clinical diagnostics, particularly for POCT requiring reliable and user-friendly glucose monitoring.

In summary, we have successfully developed a dual-modal glucose sensing platform utilizing HMPB multifunctional nanozymes, effectively addressing the long-standing issues of pH incompatibility and operational complexity in traditional enzyme-nanozymes cascade systems. The HMPB nanozymes, with their synergistic functionalities of POD-like activity, intrinsic blue coloration and photothermal properties, serve dual roles as both a catalytic activator and an intrinsic signal reporter. Specifically, the pH-independent POD-like activity of HMPB nanozymes enables direct integration with GOx without intermediate pH adjustment, thereby facilitating one-step glucose detection and representing a significant advancement over conventional multi-step protocols. Meanwhile, the intrinsic blue coloration and photothermal properties of HMPB nanozymes support dual-modal signal readout

with enhanced performance. The self-chromogenic feature, combined with the intrinsic blue coloration, promotes the generation of vivid multicolorimetric responses through the catalytic coupling of 4-AAP and phenol oxidation products, providing an enhanced colorimetric readout suitable for smartphone-based quantitative analysis. Additionally, the photothermal properties of the HMPB nanozymes, coupled with the thermal responsiveness of oxTMB, establish a dual-amplified photothermal readout for quantitative analysis based on near-infrared imaging. This dual-modal glucose sensing platform is proven to be simple, efficient, practical, and user-friendly, offering a simple POCT solution based on the enzyme-nanozymes cascade system.

Ethical statement

Human serum specimens were collected from volunteers at Hospital 940 of PLA Joint Logistics Support Force, Lanzhou, China. We state that all experiments were performed in accordance with the principles of the Helsinki Declaration, and approved by the ethics committee at Northwest Normal University and Hospital 940 of PLA Joint Logistics Support Force (No. 2022KYLL076), and informed consent was obtained from the volunteers participating in the present study.

Declaration of competing interest

The authors declare that they have no known competing financial interests or personal relationships that could have appeared to influence the work reported in this paper.

CRediT authorship contribution statement

Mingyue Luo: Writing – original draft, Validation, Methodology, Investigation, Formal analysis, Data curation, Conceptualization. **Xin Xue:** Investigation, Formal analysis, Data curation, Conceptualization. **Kehui Zhang:** Investigation, Formal analysis. **Honghong Rao:** Validation, Resources, Funding acquisition, Data curation. **Baodui Wang:** Validation, Investigation. **Zhentong Zhu:** Validation, Investigation, Conceptualization. **Jinhai Fan:** Validation, Methodology. **Zhonghua Xue:** Writing – review & editing, Supervision, Resources, Project administration, Methodology, Funding acquisition, Formal analysis, Conceptualization.

Acknowledgments

This work was supported by the National Natural Science Foundation of China (No. 22064014), Central Guided Local Science and Technology Development Fund Project (No. 25ZYJA005), the Industrial Support Program for Higher Education Institutions Project (Nos. 2023CYZC-69, 2024CYZC-05), the Science and Technology Development Plan Project of Lanzhou (No. 2021–1–146).

Supplementary materials

Supplementary material associated with this article can be found, in the online version, at doi:10.1016/j.cclet.2025.111496.

References

[1] Y. Fu, D. Zeng, J. Chao, et al., J. Am. Chem. Soc. 135 (2013) 696–702.
[2] X. Sun, Y. Li, Q. Yang, et al., Chin. Chem. Lett. 32 (2021) 1780–1784.
[3] H. Wei, E. Wang, Chem. Soc. Rev. 42 (2013) 6060–6093.
[4] S. Li, Z. Chen, F. Yang, W. Yue, Chin. Chem. Lett. 35 (2024) 108793.
[5] N. Ye, S. Huang, H. Yang, et al., Anal. Chem. 93 (2021) 13981–13989.
[6] Y. Liu, R. Lv, S. Sun, et al., Chin. Chem. Lett. 33 (2022) 807–811.
[7] L. Gao, J. Zhuang, L. Nie, et al., Nat. Nanotechnol. 2 (2007) 577–583.
[8] P. Jin, S. Lin, D. Wang, et al., Chin. Chem. Lett. 36 (2025) 110916.
[9] Y. Chen, Q. Yuchi, T. Li, et al., Sensor. Actuat. B: Chem. 305 (2020) 127436.
[10] X. Wang, L. Qin, M. Lin, H. Xing, H. Wei, Anal. Chem. 91 (2019) 10648–10656.
[11] A. Kanwal, B. Saif, A. Muhammad, et al., ACS Appl. Nano Mater. 6 (2023) 4734–4746.
[12] J. Zhang, J. Wang, J. Liao, et al., ACS Appl. Mater. Inter. 13 (2021) 50236–50245.
[13] Y. He, X. Li, X. Xu, J. Pan, X. Niu, J. Mater. Chem. B 6 (2018) 5750–5755.
[14] M.R. Krishnendu, S. Bhagat, V. Jain, D. Mehta, S. Singh, Colloid. Surface B 245 (2025) 114303.
[15] R. Zhang, L. Liu, W. Li, X. Luo, F. Wu, Colloid. Surface B 222 (2023) 113125.
[16] X. Hai, X. Zhu, K. Yu, et al., Biosens. Bioelectron. 192 (2021) 113544.
[17] W. Zhang, S. Hu, J.J. Yin, et al., J. Am. Chem. Soc. 138 (2016) 5860–5865.
[18] G. Fu, Y. Zhu, K. Xu, et al., Anal. Chem. 91 (2019) 13290–13296.
[19] X. Xue, M. Gao, H. Rao, et al., Anal. Chim. Acta 1105 (2020) 197–207.
[20] V. Krishnamoorthy, S. Rajiv, A.C.S. Sustain, Chem. Eng. 5 (2017) 146–152.
[21] W. Wang, Y. Gang, J. Peng, et al., Adv. Funct. Mater. 32 (2022) 2111727.
[22] L. Hu, H. Liao, L. Feng, M. Wang, W. Fu, Anal. Chem. 90 (2018) 6247–6252.
[23] Y.W. Bao, X.W. Hua, H.H. Ran, J. Zeng, F.G. Wu, J. Mater. Chem. B 7 (2019) 296–304.
[24] Q. Ye, E. Yuan, J. Shen, et al., Adv. Sci. 10 (2023) 2304149.
[25] W. Shi, M. He, W. Li, et al., ACS Appl. Nano Mater. 4 (2021) 802–810.
[26] S. Ning, Z. Zhang, Y. Ren, et al., Adv. Sci. 12 (2025) 2414734.
[27] R. Yin, W. Guo, H. Wang, et al., Chem. Eng. J. 334 (2018) 2539–2546.
[28] M. Hu, S. Furukawa, R. Ohtani, H. Sukegawa, et al., Angew. Chem. Int. Ed. 51 (2012) 984–988.
[29] J. Huang, H. Gu, G. Wang, et al., Anal. Chem. 95 (2023) 9107–9115.
[30] T.D. Tran, P.T. Nguyen, T.N. Le, M.I. Kim, Biosens. Bioelectron. 182 (2021) 113187.
[31] Y.S. Alqahtani, A.M. Mahmoud, M.M. El-Wekil, Talanta 253 (2023) 124024.
[32] S. Wu, D. Guo, X. Xu, J. Pan, X. Niu, Sensor Actuat. B: Chem. 303 (2020) 127225.